Advances in Physics: X

ISSN: (Print) 2374-6149 (Online) Journal homepage: https://www.tandfonline.com/loi/tapx20

# 1 / *f* noise in van der Waals materials and hybrids

Paritosh Karnatak, Tathagata Paul, Saurav Islam & Arindam Ghosh

**To cite this article:** Paritosh Karnatak, Tathagata Paul, Saurav Islam & Arindam Ghosh (2017) 1 / *f* noise in van der Waals materials and hybrids, Advances in Physics: X, 2:2, 428-449, DOI: 10.1080/23746149.2017.1314192

**To link to this article:** https://doi.org/10.1080/23746149.2017.1314192



Published online: 18 Apr 2017.

ADVANCES IN PHYSICS: X, 2017
VOL. 2, NO. 2, 428–449
https://doi.org/10.1080/23746149.2017.1314192

Taylor & Francis
Taylor & Francis Group

REVIEW ARTICLE

OPEN ACCESS Check for updates

# 1/*f* noise in van der Waals materials and hybrids

Paritosh Karnatak, Tathagata Paul, Saurav Islam and Arindam Ghosh

Department of Physics, Indian Institute of Science, Bangalore, India

**ABSTRACT**

The weak interlayer coupling in van der Waals solids allows isolation of individual atomic or molecular layers with remarkable electrical, optical, and structural properties. The applicability of these two dimensional materials in future electronic architectures requires a thorough understanding of the electrical transport mechanisms as well as of the factors limiting the device performance. The study of slow time-varying fluctuations in resistance, often called the $1/f$ noise, offers deep insight into the electronic transport and scattering mechanisms, and also acts as a performance benchmark. Here we review the current status on the magnitude and microscopic understanding of low-frequency $1/f$ noise in two-dimensional electronic materials, with specific focus on graphene, bismuth chalcogenides, and transition metal dichalcogenides. The noise characteristics differ significantly among these systems, and are directly influenced by the band structure, energy dispersion, and screening properties. The noise in field effect devices from van der Waals materials closely compares with or is even lower than that of conduction channels in conventional electronics. The excellent noise performance, when combined with high carrier mobility, energy efficiency and structural flexibility, renders an excellent platform for future electronic, optoelectronic, and sensor applications.

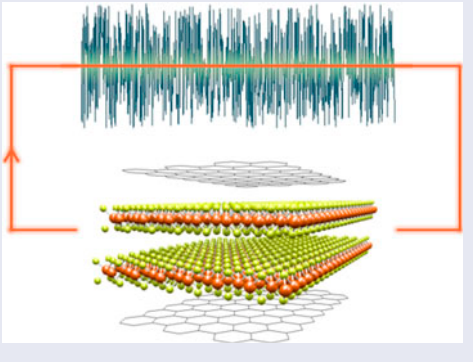

**ARTICLE HISTORY**
Received 26 January 2017
Accepted 27 March 2017

**KEYWORDS**
Low-frequency noise, graphene; transition metal dichalcogenides (TMDC); topological insulators; van der Waals heterostructures

**PACS**
73.23.-b Electronic transport in mesoscopic systems; 72.70.+m Noise processes and phenomena; 74.78.Fk Multilayers, superlattices, heterostructures; 72.10.-d Theory of electronic transport; scattering mechanisms

**CONTACT** Arindam Ghosh arindam@physics.iisc.ernet.in

## 1. Introduction

An ambitious goal in both material science and device physics is to design materials and devices with novel properties from unconventional building blocks to achieve ever improving capabilities. The isolation of graphene, a single layer of carbon atoms, from graphite in 2004 [1], seems to have provided just that opportunity. Graphene, is a remarkable material with many attributes, being, for example, the thinnest, the strongest known material, and best electrical and thermal conductor, it is also mechanically flexible and transparent [2]. Graphene has also been a platform for the discovery of many new phenomena due to its unique light-like linear energy dispersion (Figure 1(a)), and the large mobility of its charge carriers [3–5]. However, the impact of graphene is not limited to its own exceptional properties. Its discovery also led to the isolation of single or few atomic layers of a number of other materials, called the graphene analogues, which includes the transition metal dichalcogenide (TMDC) family (Figure 1(b)) [6], hexagonal boron nitride [7], and layered bismuth chalcogenides (Figure 1(c)) [8]. The common link between all these materials is the weak van der Waals force that binds their individual two-dimensional (2D) atomic or molecular layers, and hence collectively known as the van der Waals or 2D materials.

The 2D materials host a wide spectrum of physical properties, including semiconductors, superconductors, and topological insulators, hence are of interest from both fundamental and applied research perspective. In the field-effect geometry, semiconducting TMDCs exhibit lucrative properties like large ON/OFF ratio, nearly ideal subthreshold slope [9] and an immunity to short channel effects [10], making them ideal candidates for nanoelectronics, especially when the conventional technologies seem to be approaching their scaling limits (Figure 1(d)). In addition, the TMDCs are suitable for fast optical response [11–17] and exhibit valley polarization [18–22] rendering them highly suitable for optoelectronic applications. Bismuth chalcogenides, on the other hand belong to the family of topological insulators [23,24] which host topologically protected metallic surface states, while the bulk contains a semiconducting band gap. They are predicted to host Majorana fermions [25], magnetic monopoles, [26] and may be utilized for low-power electronic circuits or quantum computation [23].

While these van der Waals materials individually offer remarkable properties, they can further be combined to synthesize distinct new functionalities [13,17,27–35], serving as promising building blocks of future electronic and optoelectronic devices. One key factor that determines the device performance, and dictates the detection limits and sensitivity, is the level of low-frequency $1/f$ noise present in the system [36–44]. Although the low-frequency noise is usually undesirable which, for example, introduces phase noise in high-speed operations [41], it can also offer insights into the disorder configuration [37,38] and kinetics in the system [45,46]. Moreover, owing to the unique dimensionality of van der

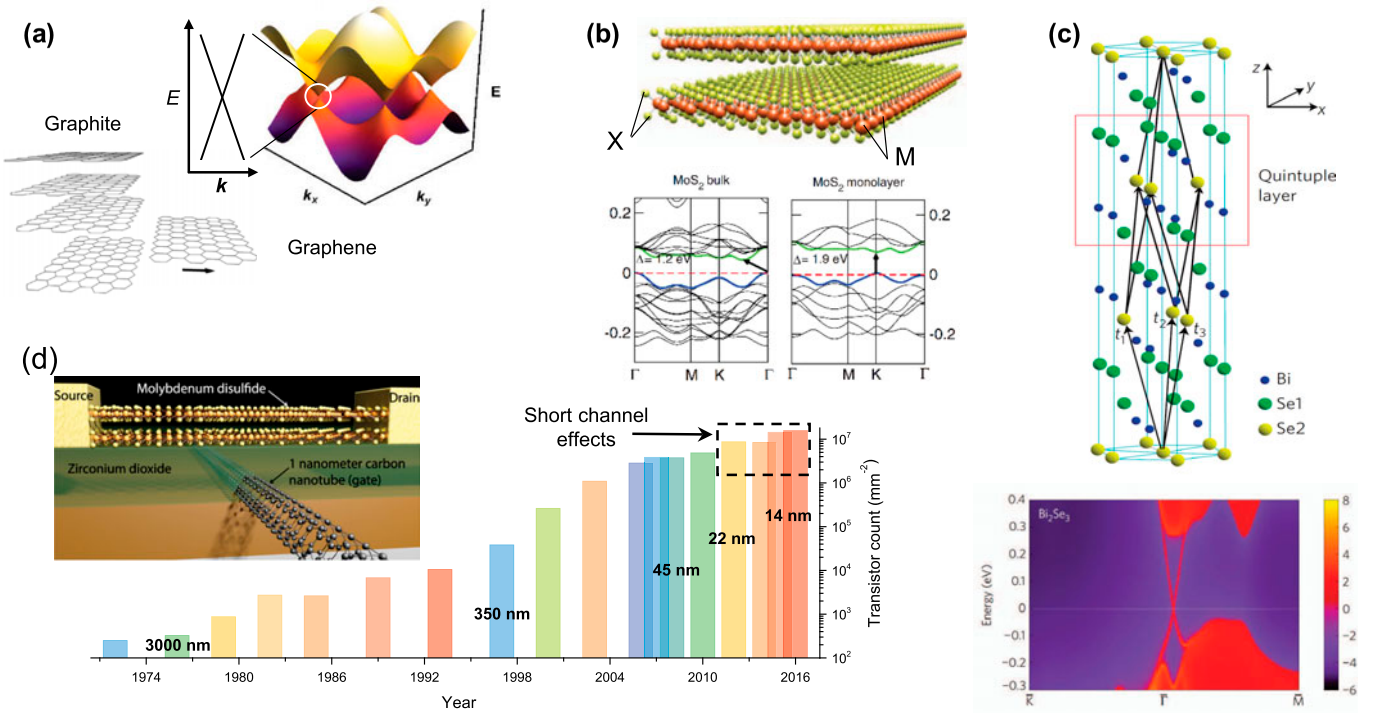


**Figure 1.** Crystal structure and band structures of (a) Graphene, (b) Transition metal dichalcogenides and (c) Bismuth Selenides. (d) Evolution of transistor count in commercial Intel CPUs demonstrating the Moore's Law.

Notes: The gate lengths are depicted by numbers on the bar graphs. A saturation in transistor count per unit area (boxed area) clearly demonstrates the limitations of silicon-based transistors due to short channel effects which can be overcome through 2D semiconductors like $MoS_2$ where an effective gate length of 1 nm has been achieved (inset). Bandstructure in part (b) is taken from Ref. [144], (c) is adapted from Ref. [8], (d) data collated from Ref. [145], inset credit: S.B. Desai, see Ref. [10].

Waals materials and their broad range of electronic properties, the study of $1/f$ noise in these materials has been of great interest [47–85].

In this review, we discuss the current state of research in three major classes of van der Waals materials, namely graphene, TMDCs, and bismuth chalcogenides. We start by briefly discussing the theoretical background for low-frequency noise that is relevant to these 2D materials, followed by highlighting the impact of non-trivial band structure in graphene and bismuth chalcogenides on the magnitude and the physics of noise. Subsequently, the noise in TMDC devices is discussed in detail. We conclude the review with a few emerging aspects of noise in van der Waals materials that establish its importance both as a unique probe to fundamental phenomena as well as in sensing and diagnostic applications.

## 2. Theoretical background

In a generic electronic device, the $1/f$ noise in the drain current is a manifestation of the slow random change in the carrier number and/or the background disorder landscape, which in turn, causes the mobility of carriers to fluctuate with time [36]. In Si-MOSFETs, for example, the carrier trapping and detrapping events at the oxide-semiconductor interface are known to constitute the dominant source of $1/f$ noise [86,87], where the traps intermittently capture electrons from the channel, and the concomitant Coulomb potential contributes to change in the carrier mobility. Due to the pure two-dimensional nature and diversity in the electronic structure of van der Waals solids, which can depend crucially on the thickness, i.e. the number of atomic/molecular layers [2,23,88], the screening of the local Coulomb trap potentials can vary widely from one system to the other (see Figure 2(a)). This causes the magnitude of noise to differ substantially between, for example, a semiconducting TMDC and semimetallic graphene that has no bandgap in the electronic structure. Below, we briefly describe the relevant theoretical framework that captures this diversity with common physical principles.

### 2.1. The $1/f$ power spectral density on noise

The ubiquity of the $1/f$-like power spectral density (PSD) of fluctuations in the electrical parameters in a solid-state system is generally attributed to slow relaxation of background disorder [89,90]. The relaxation process is a superposition of fluctuators of characteristic time $\tau$ with a distribution $D(\tau) \propto \tau^{-1}$. A single relaxation process has a power spectrum

$$S(f) \propto \frac{\tau}{(2\pi f)^2\tau^2 + 1} \tag{1}$$

The total PSD of noise is then a weighted sum of all relaxations over a bandwidth $(\tau_1,\tau_2)$,

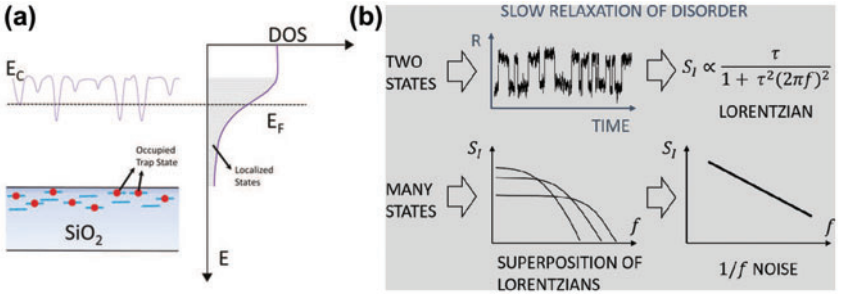


**Figure 2.** Microscopic disorder in 2D electronics and genesis of $1/f$ noise.
Note: (a) Traps in the oxide lead to spatial variation in the energy states and can lead to localization. (b) The manifestation of the $1/f$ spectrum from multiple fluctuators with a wide distribution of time scales. Figure (a) adapted from [146].

$$S(f) \propto \int_{\tau_1}^{\tau_2} \frac{\tau}{(2\pi f)^2\tau^2 + 1} D(\tau)\mathrm{d}t \tag{2}$$

which yields $S(f) \propto 1/f$, for $\tau_2^{-1} \ll f \ll \tau_1^{-1}$. Thus any random process that has a wide distribution of time scales shall exhibit a $1/f$ spectrum. The process is schematically explained in Figure 2(b).

### 2.2. Hooge model

One of the earliest and most important framework of $1/f$ noise was put forward by Hooge [36,91] where he proposed the empirical model:

$$\frac{S_V(f)}{V^2} = \frac{\gamma_H}{Nf^\alpha} \tag{3}$$

where $S_V$ is the PSD in voltage fluctuations across an electrical resistor which is biased with a constant current. Here $V$ is the average voltage drop across the sample, $N$ is total number of carriers, and $\gamma_H$ is a phenomenological dimensionless parameter, called the Hooge parameter, which gives a normalized estimate of the level of noise in a system. The frequency exponent $\alpha \approx 1 \pm 0.2$ characterizes the $1/f$ noise. Experimentally, a $1/N$ type decrease in the noise magnitude is a characteristic feature of systems following the Hooge model. The Hooge parameter varies from one system to another, and is often observed to be close to $10^{-3} - 10^{-2}$ for thin films of simple metals. This model assumes that the conductance noise originates due to mobility fluctuations which are caused by scattering of carriers due to number fluctuations of phonon modes in the lattice. Due to limited impact of disorder/impurities on mobility fluctuations, this model is applicable to homogeneous and clean metals and semiconductors.

### 2.3. Dutta–Horn model

The Dutta–Horn model [92] was first used to explain $1/f$ noise in the electrical resistance of thin metal films. In this model, slow relaxation of disorder includes

short and long-range diffusion of lattice defects and impurities [37], where the activation energy barrier $E$ to diffusion has a distribution function $D(E)$. Since the characteristic time scale $\tau = \tau_0 \exp(E/K_BT)$ is directly determined by the activation barrier, the noise magnitude

$$S(f) \propto \int_0^\infty \frac{\tau_0 \exp\left(\frac{E}{K_BT}\right)}{1 + \left(2\pi f \tau_0 \exp\left(\frac{E}{K_BT}\right)\right)^2} D(E)\mathrm{d}E \tag{4}$$

naturally assumes the $1/f$ spectral dependence, when $D(E)$ varies weakly with $E$ in the range $K_BT \ln\left(\frac{\tau_1}{\tau_0}\right) \lesssim E \lesssim K_BT \ln\left(\frac{\tau_2}{\tau_0}\right)$. Here $\tau_1^{-1}$ and $\tau_2^{-1}$ are microscopic cut-off frequency scales that are determined by, for example, finite system size or nature/spatial correlation of the disorder itself, $\tau_0^{-1}$ is the scale of phonon frequency, while $K_B$ is the Boltzmann constant. The applicability of the Dutta–Horn model can be confirmed by comparing the experimentally obtained $\alpha$ with that computed from the temperature dependence of noise. In addition, Dutta–Horn model also predicts a collapse of $fS(f)$ plotted as a function of $K_BT \ln(f/f_0)$, where $f_0 \sim 10^{13}$ Hz is the phonon frequency, for different defect densities that can be confirmed experimentally.

### 2.4. McWhorter model

The McWhorter model [86] of carrier number fluctuation was first introduced to explain the $1/f$ noise in silicon MOSFETs, where both magnitude and spectral shape of the noise were explained by the slow trapping–detrapping of charge carriers from the traps at the channel and oxide interface. The charge fluctuation results in an effective change in the surface (or gate) potential, leading to the change in carrier number in the channel. The trapping/detrapping events are described as quantum tunneling of charge between the channel and a trap state in the oxide. In such tunneling process, the characteristic relaxation time scale for a specific trap located a distance $x$ below the interface is given by, $\tau_T = \tau_0 \exp(2\kappa x)$, $\tau_0$ being a microscopic time scale of the order of the phonon frequency, and $\kappa = \sqrt{2m^*\phi_B/\hbar^2} \sim 10^9$ m$^{-1}$, where $\phi_B$ and $m^*$ are the oxide tunnel barrier height and the effective electron mass, respectively. A uniform distribution of the trap states close to the interface naturally leads to a wide distribution of $\tau_T$, which add up to $1/f$ noise in drain current $I_D$ as:

$$\frac{S_{I_D}(f)}{I_D^2} \approx \frac{e^2 K_B T}{A\kappa C_{ox}^2 f} D_{ox} \left(\frac{g_m}{I_D}\right)^2 \tag{5}$$

where $A$, $C_{ox}$, $D_{ox}$, and $g_m$ are the device area, oxide capacitance, density of oxide trap states, and transconductance, respectively. A crucial ingredient of the McWhorter model is that the gate voltage noise due to random trapping/detrapping of charge reflects in the drain current noise through transconductance

$g_m$ (as $g_m^2$) , and can be reduced by reducing the number of charge traps at the channel–substrate interface.

### 2.5. Correlated number and mobility fluctuation

One of the drawbacks of the McWhorter model was that it neglects the possibility of mobility fluctuations, which is concomitant to the trapping of charge in the gate oxide because of Coulomb scattering. This leads to an overestimation of $D_{ox}$ when the McWhorter model is used whereas in reality noise contains explicit mobility and carrier density dependence. This has been considered in Refs. [87,93], and by assuming a Coulomb scattering parameter $\alpha$, where $\alpha = \delta(\mu^{-1})/\delta N_t$ represents the change in mobility per occupied trap state, an overall expression for the PSD can be derived as,

$$\frac{S_{I_D}(f)}{I_D^2} \approx \frac{e^2 K_B T}{A\kappa f L} \int_0^L D_{ox}(E_F) \left[\frac{1}{N(y)} + \alpha\mu\right]^2 \mathrm{d}y \tag{6}$$

where $L$, $N(y)$, and $\mu$ are the channel length, charge density in the channel at a distance $y$, and carrier mobility, respectively. At low drain voltages and uniform carrier density this reduces to,

$$\frac{S_{I_D}(f)}{I_D^2} \approx \frac{e^2 K_B T}{A\kappa C_{ox}^2 f}(1 + \alpha\mu N)^2 D_{ox} \left(\frac{g_m}{I_D}\right)^2 \tag{7}$$

The correlated number-mobility fluctuation model offers a unified description of the $1/f$ noise in field-effect devices without the need to invoke a separate and often *ad hoc* bulk mobility fluctuation mechanism.

### 2.6. The generation–recombination noise and deviation from 1/f spectrum

The generation–recombination processes can also be a source of low-frequency electrical noise in electronic devices [94], in the presence of traps at a well-defined energy, for example, a narrow impurity band located at energy $\varepsilon$ below the conduction band. The relaxation rate $\tau = \tau_0 \exp(\varepsilon/K_B T)$ is the characteristic time scale of the process, and leads to a Lorentzian noise power spectrum as,

$$\frac{S_{I_D}}{I_D^2} \propto \frac{1}{1 + (2\pi f\tau)^2} \tag{8}$$

The generation–recombination noise generally appears in addition to the $1/f$ noise in the channel, and exhibits a non-monotonic $T$ dependence as the modal frequency lies within the finite measurement bandwidth in the optimal temperature range. Experimentally, it is often identified from the evolution of $f_{\max}$ with $T$, where $f_{\max} = \tau_0^{-1} \exp(-\varepsilon/K_B T)$ is the frequency at which the PSD becomes maximum.

Other models to describe various features of noise in 2D material-based field effect devices have also been suggested and highlight that the effect of charge

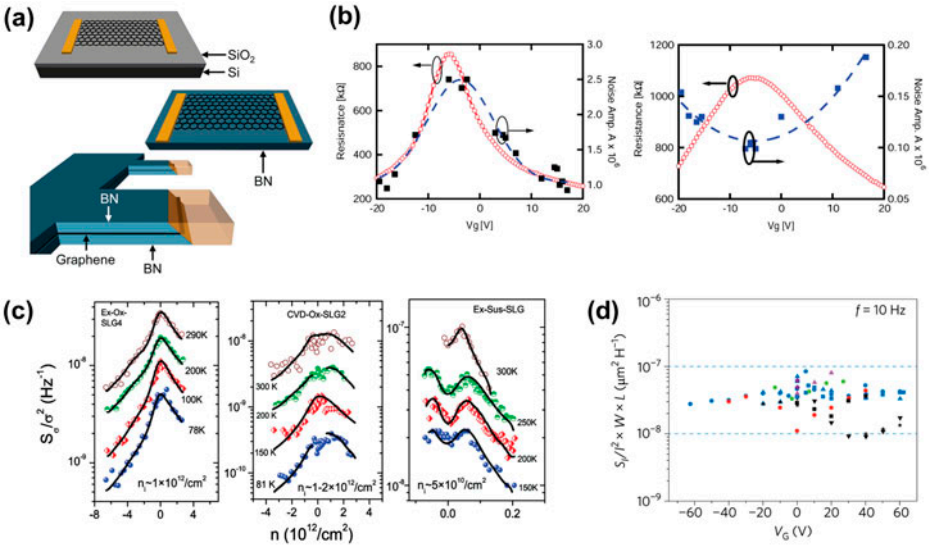


**Figure 3.** Noise in graphene.
Notes: (a) Graphene device structures, (b) Noise in single (left) and bilayer (right) graphene, (c) Noise in graphene can show different dependences on number density, (d) Noise scaling with device area, (b) is taken from Ref. [48], (c) from Ref. [53], and (d) from Ref. [62].

inhomogeneity may last upto different Fermi energy values in different materials and is dependent on their bandstructure [95,96].

## 3. Graphene

Studying $1/f$ noise in graphene is important not only from an applied perspective but is also fundamentally intriguing, for graphene hosts unique Dirac charge carriers that can be electrostatically tuned between electrons and holes along with their number density. As a result, noise has been extensively studied in graphene devices for a large range of mobility values, varying device configurations, and substrate types [47–61,63–73]. Basic graphene devices consist of graphene exfoliated typically on a 300 nm of oxide grown on top of highly doped silicon, which acts as the back gate. The contacting materials typically used are – a thin (1–10 nm) layer of a wetting metal like Cr, Ti, Pd, with Au (10–100 nm) on top to prevent oxidation. These devices display mobility values of the order of $\sim 1000$ cm$^2$V$^{-1}$s$^{-1}$ owing to the exposure of graphene to processing residues and its direct placement on $SiO_2$, which offers a rough surface with many charge traps.

Noise in such single layer graphene devices is high with the Hooge parameter ($\gamma_H$) ranging from $10^{-3}$ to $10^{-4}$ [48,53]. It is generally accepted that noise is caused by external electrostatic fluctuations, arising from the trap states in the oxide and noise is high owing to the proximity of the transport channel to the charge traps and the poor screening properties of single layer graphene. In contrast, bilayer graphene displays significantly lower $1/f$ noise (Figure 3(b))

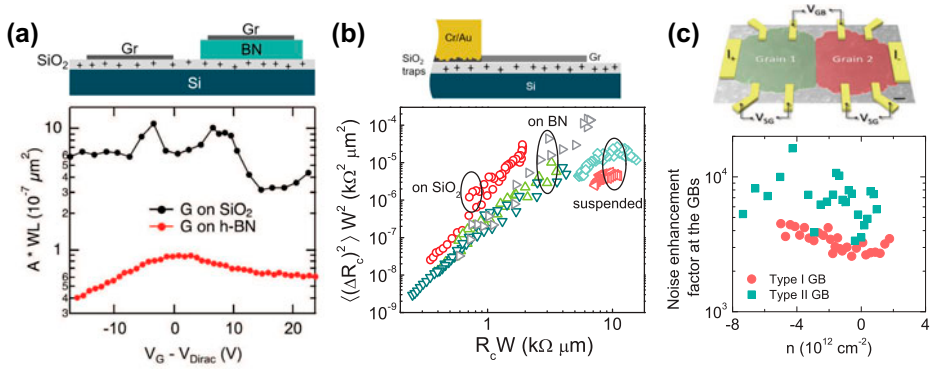


**Figure 4.** Noise mechanisms in graphene transistors.
Notes: (a) Graphene placed on BN shows lower noise than $SiO_2$ due to its separation from the oxide traps, (b) Noise scales with the fourth power of specific contact resistance indicating the contact origin of noise, (c) Noise enhancement at the grain boundaries, (a) taken from Ref. [63], (b) from Ref. [73], and (c) from Ref. [67].

than single layer graphene [48,49]. This has been attributed to the difference in their band structures and the stronger screening properties of bilayer graphene [48,49].

The exact microscopic mechanism for noise is a matter of debate and has been attributed to a combination of the number fluctuation and the mobility fluctuation model [53], or an interplay between the bandstructure and inhomogeneity [96]. While the resistance in graphene always decreases with increasing number density, noise does not always decrease monotonically with increasing carrier concentration [53] contrary to what is expected for conventional metals or semiconductors [38]. Instead, noise often shows a minima at the Dirac point and increases up to a number density value that depends on the layer number (bandstructure) and the amount of disorder present (Figure 3(c)) [53]. This has been attributed to the charge inhomogeneity near the charge neutrality point [57,95] or the interplay of short-range and long-range disorder [55]. It has been reported recently that this anomalous behavior depends on the bias applied may occur due to the pinning of electron-hole puddle [97]. While oxide traps are responsible for noise in graphene in the high-temperature range (80–300 K), at lower temperatures (< 50 K) quantum interference of Dirac carriers determines the magnitude of low-frequency noise [98–100], and increased sensitivity on defect motion may lead to an increase in noise with decreasing temperature [72]. Apart from the oxide traps, water vapor has also been shown to affect the noise generated [55] but it is not clear what role do other impurities, like resist residues and adsorbates play in the generation of flicker noise. Noise in low-mobility graphene devices also scales with the device area (Figure 3(d)), indicating the channel origin of noise [50].

To reduce the effects due to the proximity of the oxide, graphene can be suspended between two metal contacts, by wet etching of the oxide underneath, to obtain excellent electronic quality. Such suspended graphene structures exhibit

low noise ($\gamma_H \sim 10^{-5}$) [56] due to the removal of the oxide substrate from underneath the channel and partially the contacts as well. Significant further advancement in graphene electronics was achieved by the realization that hexagonal boron nitride (BN) acts as an excellent substrate to graphene [7]. BN has a similar structure as that of graphite, has few defects and can be exfoliated to reveal an atomically flat, pristine surface for the placement of graphene [7]. Further improvement can be made by encapsulating graphene between two BN crystals and making one-dimensional electrical contacts [101,102] by etching away the BN [103]. Since graphene on BN is separated from the charge traps, it shows 10–100 times lower noise (with $\gamma_H \sim 10^{-4}$) than graphene channels on the $Si/SiO_2$ substrate (Figure 4(a)) [63,64,73]. It has also been shown that in moiré superlattices, formed by aligning graphene on BN, one can attain unique noise characteristics for the cloned Dirac cones [68]. Ultralow noise devices can also be made from few and multilayer graphene, given their superior screening abilities [52] which may be suitable for interconnect applications.

### 3.1. Contact noise

Contacts have long been known to cause significant noise in devices [40,42,43,104] and can especially affect atomically thin materials by chemically reacting and altering their bandstructure to reduce their ability to screen external potential fluctuations [105,106]. It has been recently observed that for high carrier mobility graphene devices noise is entirely generated at the contacts, which depends on the contact material and contacting geometry; however, the channel characteristics such as the mobility value play little or no role (Figure 4(b)) [73]. The current crowding effect [43,107–111] which occurs due to the resistivity mismatch between the metal and graphene underneath causes a large potential drop at the contact edge and further increases the contact contribution to noise.

### 3.2. CVD graphene

Exfoliated graphene yields only micron-sized graphene, while chemical vapor deposition (CVD) of graphene offers a viable route for the creation of large-scale graphene [112]. However, the CVD-grown graphene may contain many defects and grain boundaries. These grain boundaries host short-range defects that scatter charge carriers causing a mixing of valleys, and localization of carriers [66]. It has been shown that noise from a grain boundary region can be about four orders of magnitude higher than that across a single grain (Figure 4(c)), indicating the diminished ability to screen the fluctuating (external) electrostatic potential near the grain boundary [67]. By scanning noise techniques, it has also been shown that noise sources are primarily active at the grain boundaries or at the edges [70].

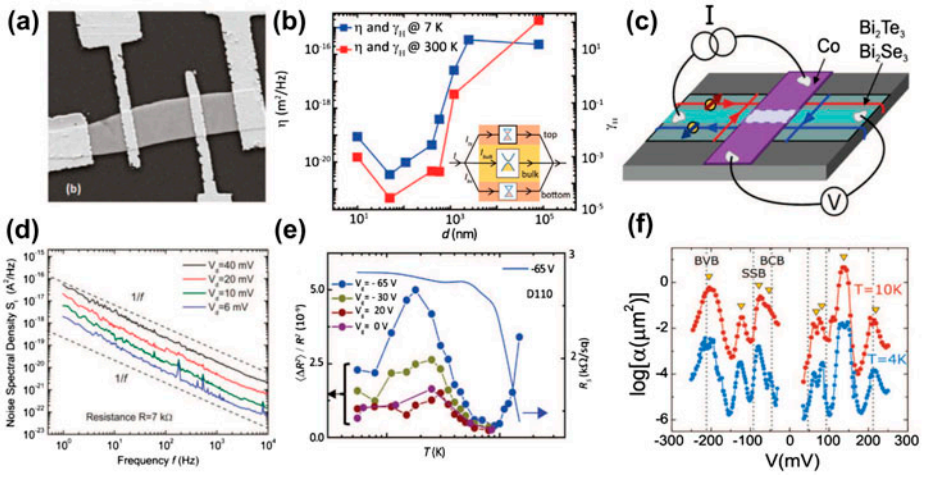


**Figure 5.** Noise in bismuth chalcogenide alloys.
Notes: (a) A typical four terminal FET from exfoliated bismuth selenide-based topological insulators (TI), (b) Power spectral density as a function of frequency as a function of sample bias. The dashed line shows $1/f$ spectra, (c) Area normalized noise parameter $\eta$ and Hooge parameter $\gamma_H$ are shown for 300 and 7 K. The phenomenological Hooge parameter for device D50 is $\approx 10^{-4}$ even at room temperature which makes it a suitable component for low noise electrical circuits, (d) Normalized noise magnitude and sheet resistance $R_S$ of exfoliated TI as a function of $T$ at different gate voltages, (e) Device schematic for $1/f$ noise measurements in a TI-based tunnel junction, (f) Noise as a function of bias is correlated with the inflection points in conductance and the band features(dashed line) for $Bi_2Te_3$ tunnel junctions. Figures reproduced from: (a)–(b) Ref. [83] (c)–(d) Ref. [81] (e)–(f) Ref. [126].

## 4. Bismuth chalcogenides

The Bismuth chalcogenide-based topological insulators (TI) [23,24,113] are among the promising 2D materials for electronic and spintronic applications due to topologically protected spin-polarized surface states. The primary challenge towards the application of this system in electronic devices arises from the chalcogen vacancies, for example, Se and Te vacancies in $Bi_2Se_3$ [114–116] and $Bi_2Te_3$ [117], respectively, which places the Fermi energy in the bulk conduction or valence bands. Several proposals to overcome this difficulty have been suggested, the most notable one being the use of multi-component alloys, such as $Bi_xSb_{2-x}Te_ySe_{3-y}$, where compensation doping quenches conduction through the bulk to a significant extent [118,119]. Nevertheless, Coulomb scattering from such impurities limits the mobility of charge carriers in surface transport [120].

The proximity and possible hybridization [121–123], of metallic surface states and semiconducting bulk states, make noise characteristics in TI [81–83] differ significantly from that in graphene. While the substrate plays a major role in determining the noise magnitude in graphene [49,53], the $1/f$ noise in TI can have a very different origin even though the basic device structure remains the same (Figure 5(a)). The key challenge has been to isolate the noise in surface transport from that in the bulk. Early noise measurements [83] in exfoliated nanoflakes of $Bi_2Se_3$ at room temperature, which clearly demonstrated noise PSD $\propto 1/f^{\alpha}$ with $\alpha = 1.11 \pm 0.02$ (Figure 5(b)), did not differentiate between the surface and bulk contributions.

Recently Bhattacharyya et al. [81] have carried out extensive $1/f$ noise measurements in mechanically exfoliated $Bi_{1.6}Sb_{0.4}Te_2Se$ (BSTS) alloys on $p^{++}$ $SiO_2$/Si substrate as function of temperature ($T \sim 7 - 300$ K), film thickness ($d \approx 10$ nm to bulk), and gate voltage $V_g$. The electrical transport in these systems has been shown to be dominated by surface states for $T < 50$ K and $d \leq 1\mu$m. Both noise parameter $\eta = AS_V(f)/V^2$ and the Hooge parameter $\gamma_H$, where $A$ is the device area, were shown to depend strongly on $d$ and $T$. In Figure 5(c), the sharp increase in $\eta$ for $d \geq 1\,\mu$m at $V_g = 0$ V is directly related to the onset of bulk conduction in TI samples. However, the $V_g$ dependence of noise in a typical exfoliated TI with $d = 110$ nm shows a monotonic increase as the number density is tuned towards the charge neutrality point (CNP), or the Dirac point, for different temperatures. Due to the branching of current in three parallel paths (inset Figure 5(c)), the $V_g$ dependence of noise has been modeled using the equation:

$$\frac{\langle \triangle R^2 \rangle}{R^2} = \frac{G_t^2}{G_{\text{tot}}^2} N_t + \frac{G_{\text{bulk}}^2}{G_{\text{tot}}^2} N_{\text{bulk}} + \frac{G_b^2}{G_{\text{tot}}^2} N_b \tag{9}$$

where $N_x = \langle \triangle R_X^2 \rangle / R_X^2$ is the relative variance of noise and $x = t$, $b$ and bulk are top surface, bottom surface and bulk of the TI, respectively, and $G_{\text{tot}} = G_t + G_{\text{bulk}} + G_b = R^{-1}$ are the respective conductances. It has been shown that the mobility-fluctuation-induced noise satisfactorily describes the $V_g$ dependence where $N_x = \gamma_H^x A / n_x$, $n_x$ being the number density of respective surfaces. McWhorter type number density fluctuation model fails to describe the $V_g$ dependence both qualitatively as well as quantitatively. In thin exfoliated devices [81] of thickness ~10 nm, the $V_g$ dependence of noise shows a monotonic increase with a suppression near Dirac point which vanishes as the temperature is increased. Such $M$-type behavior has been observed in graphene as well [53] and has been predicted to originate from mesoscopic quantum interference effect in Dirac fermions in a spatially inhomogeneous carrier distribution [124].

The $T$-dependence of noise in TI (Figure 5(d)) was found to be unique amongst different classes of 2D materials, and reveals a series of unexpected peaks at characteristic temperatures irrespective of the thickness. Such peaks in semiconductors usually arise due to either generation–recombination of noise or due to diffusion of defects, although the latter involves much larger energy scale (~1 eV), and is expected to occur at higher temperatures. An in-depth analysis of the PSD close to the noise maxima reveals generation–recombination processes in the (insulating) bulk of the TI that manifest through mobility fluctuations in the surface transport. The analysis also indicated two impurity bands with $\triangle E = 20$ meV, which corresponds to Se vacancies and, $\triangle E \approx 130$ meV which is likely due to p-type (Bi,Se)/Te antisite defects [125]. It is remarkable that while the insulating bulk of the TI does not directly contribute to electrical conduction, it appears to be the dominant source of $1/f$ noise in TI-based devices.

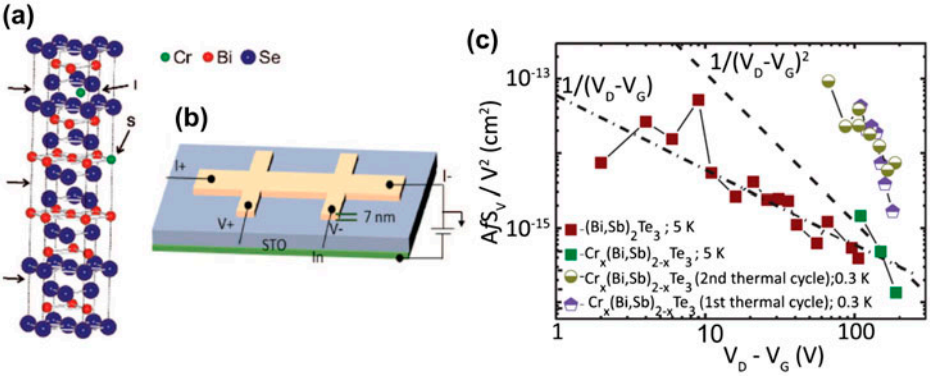


**Figure 6.** Noise in magnetically doped topological inslators.
Notes: (a) The crystal structure of chromium doped $Bi_2Se_3$. Cr is present either as an interstitial element or substitutes a Bi in the lattice [147]. (b) Schematic of device used for noise measurements in [82]. The Cr-doped Tl film is shaped in Hall bar configuration on SrTiO−3 (STO) substrate. (c) Area normalized noise for molecular beam epitaxy (MBE) grown samples are shown for different thermal cycles measured from the Dirac point: Figures reproduced from: (a) Ref. [147], (b)–(c) Ref. [82].

The effect of bandstructure of TIs has also been investigated by measuring $1/f$ spectra [126] in perpendicular tunnel junctions. In Figure 5(e), the device geometry consisting of a bottom electrode of MBE grown $Bi_2Se_3/Bi_2Te_3$ and Co with $Al_2O_3$ as a tunnel barrier is shown. The $1/f$ noise spectra reveals a series of peaks as function of a bias voltage which also agrees with the inflection points in the conductance. While the peak at $\pm 200$ mV is close to the bulk valence band for $Bi_2Te_3$, the other peaks can originate due to the availability of the transport channels in the surface state band and bulk conduction band.

The microscopic origin of noise in MBE grown undoped TI $(Bi,Sb)_2Te_3$ and ferromagnetically doped TI (FMTI) $Cr_x(Bi,Sb)_{2-x}Te_3$ on STO substrate (Figure 6(a) and (b)) has been investigated in Ref. [82]. In Figure 6(c), the $V_D$-$V_G$ dependence of noise has been shown, where $V_D$ is the Dirac point gate voltage. The area normalized $1/f$ noise in the undoped samples shows a $1/(V_D\text{-}V_G)$ dependence, while the FMTI shows a much stronger dependence than Hooge mobility fluctuation ($\sim 1/V_D\text{-}V_G$) or Mcwhorter number-fluctuation $\sim 1/(V_G - V_D)^2$. The $T$ dependence of noise in FMTI has also been investigated in Ref. [82]. Both $V_g$ and $T$ dependences seem to indicate noise processes in the localized regime, for example, that arising in the Efros–Shklovskii variable range hopping transport. Since the magnetic impurities break time reversal symmetry, thereby destroying the topological protection to localization, the conduction occurs inherently along the bulk of the film, and possibly in the impurity bands formed by the Cr dopants.

## 5. Transition metal dichalcogenides

Low-frequency noise in mechanically exfoliated TMDC field effect transistors on $SiO_2$ substrates has very different characteristics from that observed in graphene

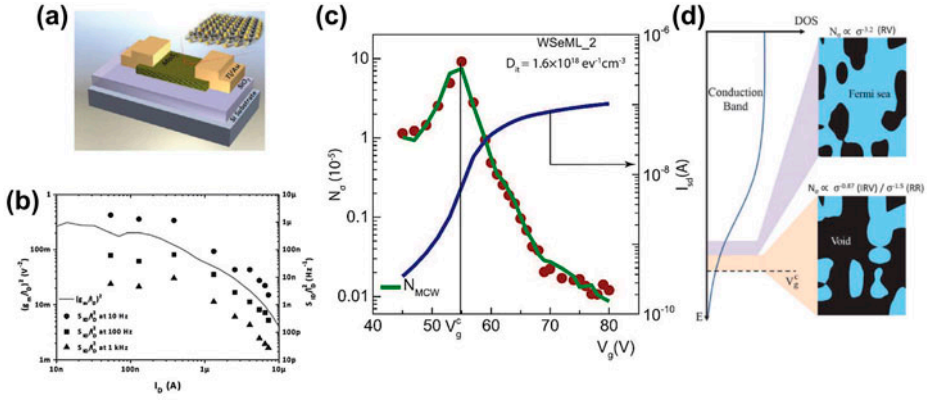


**Figure 7.** Noise in transition metal dichalcogenide field-effect transistors.
Notes: (a) Schematic depiction of a typical $SiO_2$ backgated $MoS_2$ FET. (b) Scaling of normalized transconductance $(g_m/I_D)^2$ and PSD $S_{ID}/I_D^2$ with drain current $I_D$ for the device in part (a). (c) Plots of experimentally measured normalized integrated PSD (wine colored dots), theoretically computed noise magnitude using McWhorter model (olive colored line) and drain current $I_{sd}$ (navy blue colored line) with gate voltage $V_g$. Substrate trap density $D_{it}$ was used as a parameter for plotting the theoretical noise values. The qualitative and quantitative agreement of these plots using experimental range of $D_{it}$ values proves the McWhorter origin of noise. (d) Schematic depicting the microscopic state of a TMDC channel near percolation threshold $V_g^c$ durin ON-OFF transition. Part (a) and (b) are taken from Ref. [78], (c) and (d) are from Ref. [79].

or the bismuth chalcogenide-based topological insulators. This is not surprising given the semiconducting band structure in many of these systems (Figure 1), which strongly suppresses the screening of environmental Coulomb scatterers. Early noise measurements [78] in $MoS_2$ and $WSe_2$ FETs reported decrease of the noise magnitude (Hooge parameter) with increasing gate voltage $V_g$ or channel current $I_D$, in a manner that closely followed the McWhorter number-fluctuation model [86] (Equation (5), Figure 7(b)). This was later confirmed by several groups [74,76,79,127], and a direct correlation between the noise magnitude and $(g_m/I_D)^2$, where $g_m$ and $I_D$ are the transconductance and drain current, respectively (Figure 7(c)), conclusively established that random intermittent exchange of charge between the TMDC channel and charge traps on the $SiO_2$ surface is the dominant source of $1/f$ noise in these devices.

However, noise measurements in exfoliated TMDC layers on $SiO_2$ fail to clarify two important issues: (1) role of surface traps as opposed to those at the $SiO_2$ interface, and (2) the role of the TMDC-metal contacts. It is now established that the electrical transparency of the metal-TMDC contacts is crucial to high carrier mobility in TMDC FETs, and large improvement in mobility is observed on annealing the contacts at elevated temperatures prior to measurement [128–130]. The extent of contact noise was first considered in Ref. [76], although latter reports of absence of area scaling [79] and possible impact of surface adsorbants [77] prevented an unambiguous separation of the channel and contact contribution to noise. To resolve these issues, a series of van der Waals heterostructures with partial encapsulation of the TMDC ($MoS_2$) channel by hexagonal boron nitride (BN) were studied in Ref. [74]. The regions covered

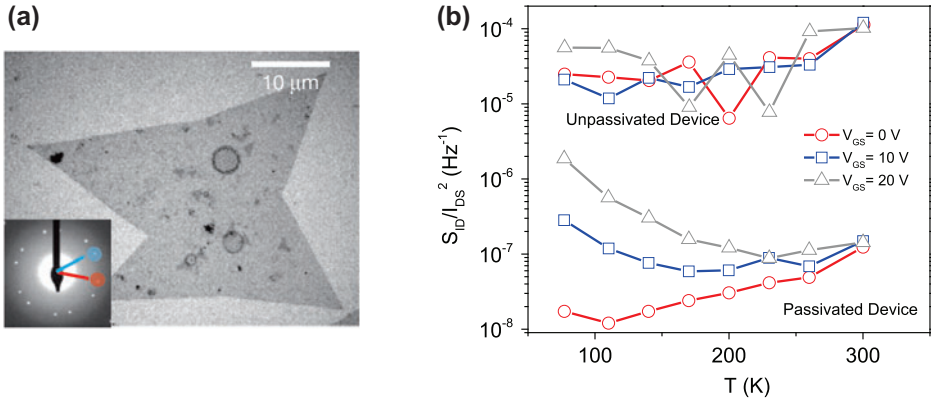


**Figure 8.** Noise in chemical vapor deposited (CVD) TMDC devices.
Notes: (a) TEM image of CVD grown $MOS_2$ is taken from Ref. [135]. (b) Comparison of temperature dependence of noise magnitude in $Al_2O_3$ passivated and unpassivated CVD $MoS_2$ data taken from Ref. [140].

by BN remained protected from polymeric and atmospheric contaminants. No significant difference in the noise magnitude between the BN-protected and exposed parts of the channels could be observed, although a large decrease in noise was observed on annealing. These evidences indicate a strong contribution of contact noise in un-annealed devices, while channel noise dominates when the contacts are annealed [79].

In a recent development, Fang et al. [80] reported a study of random telegraphic signals at low temperatures. These experiments reveal the impact of isolated defects in the $MoS_2$ channel, as well as that of defect-defect interactions, on the observed RTS. In another work, Paul et al. [79] employed $1/f$ noise magnitude to probe the microscopic mechanism of electrical transport at ON-OFF transition, or switching, in TMDC FETs. They report a scaling of the noise magnitude with average conductivity, characterized by universal scaling exponents [131–133], which suggests inhomogeneous charge distribution in TMDC FETs at the switching transition, and a dynamic evolution of classical percolative transport from the inverted random void (weakly-connected puddles) to the random void (island-in-sea) regimes (Figure 7(d)).

Noise measurements have now been carried out in CVD-grown TMDC systems as well, where the lattice defects (such as, vacancies) and grain boundaries [134,135] act as scattering centers, in addition to charged traps at substrate interface. The scenario is further complicated by the modification in the band structure, which impacts both electronic and magnetic properties, by localized and extended defects (grain boundaries) in 2D system [136–139]. Noise in single grain regions of CVD $MoS_2$ FETs [140] is found to be sensitive to the dielectric environment with a large decrease in the normalized PSD observed on surface passivation with $Al_2O_3$ (Figure 8(b)). Current fluctuations, however, continue follow a correlated number and mobility fluctuation model as discussed previously.

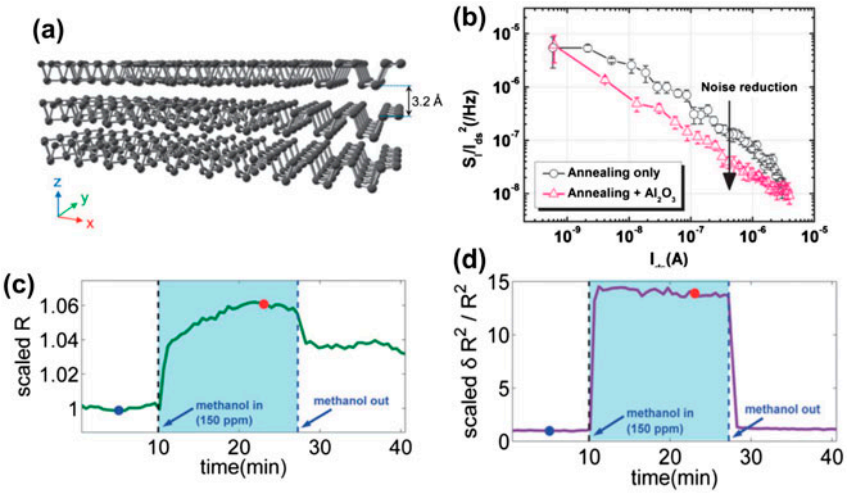


**Figure 9.** Noise in black phosphorus and emerging applications.
Notes: (a) Schematic depiction of three layers of black phosphorous. (b) Comparison of normalized power spectral density in black phosphorous FETs before and after passivation with $Al_2O_3$. Change in resistance (c) and channel noise (d) of a graphene transistor on exposure to methanol vapor. The values of resistance and electronic noise are normalized by their respective values in the pristine device. Subsection (a) and (b) are taken from Ref. [84] while (c) and (d) are from Ref. [143].

## 6. Emerging applications and conclusion

### 6.1. Noise in black phosphorus

Black phosphorus (BP) is a thermodynamically stable gapped allotrope of phosphorus, and an emerging member of the ultra-thin material family. A single layer of BP has a linked chain of phosphorous atoms forming a puckered honeycomb sheet as shown in (Figure 9(a)). It has a 2 eV single layer bandgap which reduces to 0.3 eV for bulk BP making it one of the smallest bandgap two-dimensional semiconducting materials. Thus, few layer BP FETs are ambipolar [85,141], have high carrier mobilities (upto 1000 $cm^2V^{-1}s^{-1}$)) [141], and a large ON-OFF ratio making them suitable for logic and complementary MOS applications.

Noise measurement in BP FETS is employed to investigate the role played by interfacial traps and/or contacts on device performance [84,85]. Interestingly, the microscopic mechanism of noise seems to differ depending on the doping, where *n*-type and *p*-type doping exhibits dominance of mobility fluctuations and correlated number–mobility fluctuation noise, respectively. Annealing helps in improving the device characteristics temporarily while passivation with a high-*k* dielectric, such as $Al_2O_3$, is found to protect the channel for a longer period of time while reducing channel noise (Figure 9(b)), hysteresis and improving the field effect mobility and subthreshold slope [84].

### 6.2. Noise as a sensor

The large surface-to-volume ratio of 2D materials makes them very sensitive to the surrounding environment. This has enabled $1/f$ noise measurements in

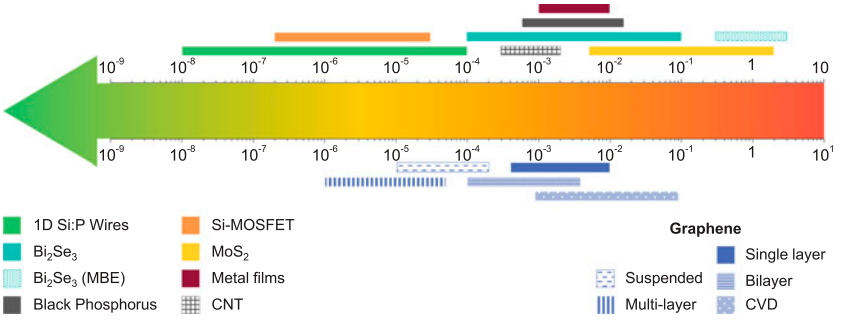


**Figure 10.** Hooge parameters for various low-dimensional systems, and comparison with that in 2D materials.
Notes: Collated from [48,52,53,56,68,77,81,83,85,148–150].

graphene FETs to determine the presence of environmental chemical species, such as, methanol, nitrobenzene, chloroform, and ammonia [142,143]. Both channel resistance and noise magnitude increase when graphene FETs are exposed to vapor of such chemicals, but compared to a 6% change in electrical resistance, the change in the noise magnitude on exposure to chemical analytes is ~1500% (Figure 9(c) and (d)) [143]. The resetting time for noise-based sensors is also found to be considerably lower than that of a resistance-based sensor making it a far superior probe for gas-sensing application. Moreover, the adsorbates interact with graphene with chemical-specific characteristic frequencies, causing the noise power spectrum to deviate from pure $1/f$ behavior. This may allow specificity in chemical sensing.

Low-frequency noise has been widely utilized to study the physics of resistance fluctuations in van der Waals materials. Their dimensionality and unconventional electronic structures uniquely affect the physics of resistance fluctuations. However, there remains a lot to look forward to, for despite extensive investigation, a more refined understanding of the microscopic mechanism of noise in these materials is desirable. Noise may also aid in addressing some fundamental questions on localization physics and edge modes, as noise is sensitive to the bandstructure, the local density of states, and the disorder landscape, especially in systems like bilayer graphene that offer a readily accessible and rich phase space.

Noise has also been employed as a diagnostic tool to gauge the performance limiting factors in van der Waals materials. These investigations indicate that in all van der Waals materials, with the exception of exfoliated graphene, resistance fluctuations are enhanced or even generated by intrinsic defects. This calls for a perfection toward the high-quality growth of these materials. Developing superior electrical contacts is another important direction toward improving their noise performance. To quantify how van der Waals materials currently compare with alternate emerging materials and conventional materials the Hooge parameter, a figure of merit for noise is shown in Figure 10. The class of van der Waals materials also continues to expand rapidly, and we may expect new

materials with superior noise characteristics. Finally, the sensitivity of noise magnitude to external stimuli, coupled with the unique electronic properties of two dimensional materials makes them ideal candidates for sensor applications.

In conclusion, van der Waals materials are currently at the forefront of research, being explored for novel physical phenomena and for their application potential. Their applicability in novel and high-quality electronic and optoelectronic applications will crucially depend on minimizing the resistance noise.

## Disclosure statement

The authors declare no conflict of interest.

## References

[1] K.S. Novoselov, A.K. Geim, S. Morozov, D. Jiang, Y. Zhang, S. Dubonos, I. Grigorieva and A. Firsov, Science 306 (2004) p.666.
[2] A.H. Castro Neto, F. Guinea, N.M.R. Peres, K.S. Novoselov and A.K. Geim, Rev. Mod. Phys. 81 (2009) p.109–162.
[3] Y. Zhang, Y.-W. Tan, H.L. Stormer and P. Kim, Nature 438 (2005) p.201.
[4] G.-H. Lee, G.-H. Park and H.-J. Lee, Nat. Phys. 11 (2015) p.925.
[5] D. Bandurin, I. Torre, R.K. Kumar, M.B. Shalom, A. Tomadin, A. Principi, G. Auton, E. Khestanova, K. Novoselov, I. Grigorieva, et al., Science 351 (2016) p.1055.
[6] K.F. Mak, C. Lee, J. Hone, J. Shan and T.F. Heinz, Phys. Rev. Lett. 105 (2010) p.136805.
[7] C. Dean, A. Young, I. Meric, C. Lee, L. Wang, S. Sorgenfrei, K. Watanabe, T. Taniguchi, P. Kim, K. Shepard, et al., Nat. Nanotechnol. 5 (2010) p.722.
[8] H. Zhang, C.-X. Liu, X.-L. Qi, X. Dai, Z. Fang and S.-C. Zhang, Nat. Phys. 5 (2009) p.438.
[9] B. Radisavljevic, A. Radenovic, J. Brivio, V. Giacometti and A. Kis, Nat. Nanotechnol. 6 (2011) p.147.
[10] S.B. Desai, S.R. Madhvapathy, A.B. Sachid, J.P. Llinas, Q. Wang, G.H. Ahn, G. Pitner, M.J. Kim, J. Bokor, C. Hu, et al., Science 354 (2016) p.99.
[11] O. Lopez-Sanchez, D. Lembke, M. Kayci, A. Radenovic and A. Kis, Nat. Nanotechnol. 8 (2013) p.497.
[12] K. Roy, M. Padmanabhan, S. Goswami, T.P. Sai, S. Kaushal and A. Ghosh, Solid State Commun. 175–176 (2013) p.35.
[13] K. Roy, M. Padmanabhan, S. Goswami, T. Sai, G. Ramalingam, S. Raghavan and A. Ghosh, Nat. Nanotechnol. 8 (2013) p.826.
[14] B.W.H. Baugher, H.O.H. Churchill, Y. Yang and P. Jarillo-Herrero, Nat. Nanotechnol. 9 (2014) p.262.
[15] A. Pospischil, M.M. Furchi and T. Mueller, Nat. Nanotechnol. 9 (2014) p.257.
[16] J.S. Ross, P. Klement, A.M. Jones, N.J. Ghimire J. Yan, M.G.T. Taniguchi, K. Watanabe, K. Kitamura, W. Yao et al., Nat. Nanotechnol. 9 (2014) p.268.
[17] C.H. Lee, G.-H. Lee, A.M. van der Zande, W. Chen, Y. Li, M. Han, X. Cui, G. Arefe, C. Nuckolls, T.F. Heinz, et al., Nat. Nanotechnol. 9 (2014) p.676.
[18] K.F. Mak, K.L. McGill, J. Park and P.L. McEuen, Science 344 (2014) p.1489.
[19] K.F. Mak, K. He, J. Shan and T.F. Heinz, Nat. Nanotechnol. 7 (2012) p.494.
[20] A.M. Jones, H. Yu, N.J. Ghimire, S. Wu, G. Aivazian, J.S. Ross, B. Zhao, J. Yan, D.G. Mandrus, D. Xiao, et al., Nat. Nanotechnol. 8 (2013) p.634.
[21] Q. Wang, S. Ge, X. Li, J. Qiu, Y. Ji, J. Feng and D. Sun, ACS Nano 7 (2013) p.11087.

[22] J. Kim, X. Hong, C. Jin, S.-F. Shi, C.-Y.S. Chang, M.-H. Chiu, L.-J. Li and F. Wang, Science 346 (2014) p.1205.
[23] M.Z. Hasan and C.L. Kane, Rev. Mod. Phys. 82 (2010) p.3045.
[24] Y. Ando, J. Phys. Soc. Jpn. 82 (2013) p.102001.
[25] L. Fu and C.L. Kane, Phys. Rev. Lett. 100 (2008) p.096407.
[26] X.-L. Qi, R. Li, J. Zang and S.-C. Zhang, Science 323 (2009) p.1184.
[27] L. Britnell, R. Ribeiro, A. Eckmann, R. Jalil, B. Belle, A. Mishchenko, Y.-J. Kim, R. Gorbachev, T. Georgiou, S. Morozov, et al., Science 340 (2013) p.1311.
[28] W.J. Yu, Y. Liu, H. Zhou, A. Yin, Z. Li, Y. Huang and X. Duan, Nat. Nanotechnol. 8 (2013) p.952.
[29] T. Georgiou, R. Jalil, B.D. Belle, L. Britnell, R.V. Gorbachev, S.V. Morozov, Y.-J. Kim, A. Gholinia, S.J. Haigh, O. Makarovsky, et al., Nat. Nanotechnol. 8 (2013) p.100.
[30] G.H. Lee, Y.-J. Yu, X. Cui, N. Petrone, C.-H. Lee, M.S. Choi, D.-Y. Lee, C. Lee, W.J. Yoo, K. Watanabe, et al., ACS Nano 7 (2013) p.7931.
[31] P. Rivera, J.R. Schaibley, A.M. Jones, J.S. Ross, S. Wu, G. Aivazian, P. Klement, K. Seyler, G. Clark, N.J. Ghimire, et al., Nat. Commun. 6 (2015) p.6242.
[32] P. Rivera, K.L. Seyler, H. Yu, J.R. Schaibley, J. Yan, D.G. Mandrus, W. Yao and X. Xu, Science 351 (2016) p.688.
[33] X. Hong, J. Kim, S.-F. Shi, Y. Zhang, C. Jin, Y. Sun, S. Tongay, J. Wu, Y. Zhang and F. Wang, Nat. Nanotechnol. 9 (2014) p.682.
[34] W.J. Yu, Z. Li, H. Zhou, Y. Chen, Y. Wang, Y. Huang and X. Duan, Nat. Mater. 12 (2013) p.246.
[35] A.K. Geim and I.V. Grigorieva, Nature 499 (2013) p.419.
[36] F. Hooge, Phys. Lett. A 29 (1969) p.139.
[37] P. Dutta and P.M. Horn, Rev. Mod. Phys. 53 (1981) p.497.
[38] M.B. Weissman, Rev. Mod. Phys. 60 (1988) p.537.
[39] B.K. Jones, AIP Conf. Proc. 511 (2000) p.115.
[40] F. Hooge and A. Hoppenbrouwers, Phys. Lett. A 29 (1969) p.642.
[41] B. Razavi, IEEE J. Solid-State Circuits 31 (1996) p.331.
[42] L. Vandamme, IEEE Trans. Electron Devices 41 (1994) p.2176.
[43] E. Vandamme and L. Vandamme, Microelectron. Reliab. 40 (2000) p.1847.
[44] S. Grover, S. Dubey, J.P. Mathew and M.M. Deshmukh, Appl. Phys. Lett. 106 (2015) p.051113.
[45] G.T. Seidler and S.A. Solin, Phys. Rev. B 53 (1996) p.9753.
[46] U. Chandni, A. Ghosh, H. Vijaya and S. Mohan, Phys. Rev. Lett. 102 (2009) p.025701.
[47] Z. Chen, Y.-M. Lin, M.J. Rooks and P. Avouris, Physica E 40 (2007) p.228.
[48] Y.-M. Lin and P. Avouris, Nano Lett. 8 (2008) p.2119.
[49] A.N. Pal and A. Ghosh, Phys. Rev. Lett. 102 (2009) p.126805.
[50] S. Rumyantsev, G. Liu, W. Stillman, M. Shur and A.A. Balandin, J. Phys. Conden. Matter 22 (2010) p.395302.
[51] Q. Shao, G. Liu, D. Teweldebrhan, A.A. Balandin, S. Rumyantsev, M.S. Shur and D. Yan, IEEE Electron Device Lett. 30 (2009) p.288.
[52] A.N. Pal and A. Ghosh, Appl. Phys. Lett. 95 (2009) p.082105.
[53] A.N. Pal, S. Ghatak, V. Kochat, E.S. Sneha, A. Sampathkumar, S. Raghavan and A. Ghosh, ACS Nano 5 (2011) p.2075.
[54] I. Heller, S. Chatoor, J. Mannik, M.A.G. Zevenbergen, J.B. Oostinga, A.F. Morpurgo, C. Dekker and S.G. Lemay, Nano Lett. 10 (2010) p.1563.
[55] A. Kaverzin, A. Mayorov, A. Shytov and D. Horsell, Phys. Rev. B 85 (2012) p.075435.
[56] Y. Zhang, E.E. Mendez and X. Du, ACS Nano 5 (2011) p.8124.

[57] G. Xu, C.M. Torres, Y. Zhang, F. Liu, E.B. Song, M. Wang, Y. Zhou, C. Zeng and K.L. Wang, Nano Lett. 10 (2010) p.3312.
[58] G. Liu, S. Rumyantsev, M.S. Shur and A.A. Balandin, Appl. Phys. Lett. 102 (2013) p.093111.
[59] G. Liu, S. Rumyantsev, M. Shur and A.A. Balandin, Appl. Phys. Lett. 100 (2012) p.033103.
[60] S. Imam, S. Sabri and T. Szkopek, IET Micro Nano Lett. 5 (2010) p.37.
[61] G. Liu, W. Stillman, S. Rumyantsev, Q. Shao, M. Shur and A. Balandin, Appl. Phys. Lett. 95 (2009) p.033103.
[62] A.A. Balandin, Nat. Nanotechnol. 8 (2013) p.549.
[63] M. Kayyalha and Y.P. Chen, Appl. Phys. Lett. 107 (2015) p.113101.
[64] M.A. Stolyarov, G. Liu, S.L. Rumyantsev, M. Shur and A.A. Balandin, Appl. Phys. Lett. 107 (2015) p.023106.
[65] M. Kumar, A. Laitinen, D. Cox and P.J. Hakonen, Appl. Phys. Lett. 106 (2015) p.263505.
[66] A.N. Pal, A.A. Bol and A. Ghosh, Appl. Phys. Lett. 97 (2010) p.133504.
[67] V. Kochat, C.S. Tiwary, T. Biswas, G. Ramalingam, K. Hsieh, K. Chattopadhyay, S. Raghavan, M. Jain and A. Ghosh, Nano Lett. 16 (2015) p.562.
[68] C. Kumar, M. Kuiri, J. Jung, T. Das and A. Das, Nano Lett. 16 (2016) p.1042.
[69] M.G. Sung, H. Lee, K. Heo, K.-E. Byun, T. Kim, D.H. Seo, S. Seo and S. Hong, ACS Nano 5 (2011) p.8620.
[70] H. Lee, D. Cho, S. Shekhar, J. Kim, J. Park, B.H. Hong and S. Hong, ACS Nano 10 (2016) p.10135.
[71] J. Moon, D. Curtis, D. Zehnder, S. Kim, D. Gaskill, G. Jernigan, R. Myers-Ward, J. Eddy, P. Campbell, K.-M. Lee et al., IEEE Electr. Device L. 32 (2011) p.270.
[72] C.-C. Kalmbach, F.J. Ahlers, J. Schurr, A. Müller, J. Feilhauer, M. Kruskopf, K. Pierz, F. Hohls and R.J. Haug, Phys. Rev. B 94 (2016) p.205430.
[73] P. Karnatak, T.P. Sai, S. Goswami, S. Ghatak, S. Kaushal and A. Ghosh, Nat. Commun. 7 (2016) p.13703.
[74] S. Ghatak, S. Mukherjee, M. Jain, D.D. Sarma and A. Ghosh, APL Mat. 2 (2014) p.092515.
[75] J. Na, M.-K. Joo, M. Shin, J. Huh, J.-S. Kim, M. Piao, J.-E. Jin, H.-K. Jang, H.J. Choi, J.H. Shim, et al., Nanoscale 6 (2014) p.433.
[76] J. Renteria, R. Samnakay, S.L. Rumyantsev, C. Jiang, P. Goli, M.S. Shur and A.A. Balandin, Appl. Phys. Lett. 104 (2014) p.153104.
[77] V.K. Sangwan, H.N. Arnold, D. Jariwala, T.J. Marks, L.J. Lauhon and M.C. Hersam, Nano Lett. 13 (2013) p.4351.
[78] H.-J. Kwon, H. Kang, J. Jang, S. Kim and C.P. Grigoropoulos, Appl. Phys. Lett. 104 (2014) p.083110.
[79] T. Paul, S. Ghatak and A. Ghosh, Nanotechnology 27 (2016) p.125706.
[80] N. Fang, K. Nagashio, and A. Toriumi, 2D Mater. 4 (2017), p.015035.
[81] S. Bhattacharyya, M. Banerjee, H. Nhalil, S. Islam, C. Dasgupta, S. Elizabeth and A. Ghosh, ACS Nano 9 (2015) p.12529.
[82] S. Bhattacharyya, A. Kandala, A. Richardella, S. Islam, N. Samarth and A. Ghosh, Appl. Phys. Lett. 108 (2016) p.082101.
[83] M.Z. Hossain, S.L. Rumyantsev, K.M. Shahil, D. Teweldebrhan, M. Shur and A.A. Balandin, ACS Nano 5 (2011) p.2657.
[84] J. Na, Y.T. Lee, J.A. Lim, D.K. Hwang, G.-T. Kim, W.K. Choi and Y.-W. Song, ACS Nano 8 (2014) p.11753.
[85] X. Li, Y. Du, M. Si, L. Yang, S. Li, T. Li, X. Xiong, P. Ye and Y. Wu, Nanoscale 8 (2016) p.3572.

[86] A. McWhorter, Semicond. Surf. Phys. (1957) p.207.
[87] R. Jayaraman, C.G. Sodini and I.E.E.E. Trans, Electron Devices 36 (1989) p.1773.
[88] Q.H. Wang, K. Kalantar-Zadeh, A. Kis, J.N. Coleman and M.S. Strano, Nat Nano. 7 (2012) p.699.
[89] M. Weissman, Rev. Mod. Phys. 60 (1988) p.537.
[90] M. Weissman, Annu. Rev. Mater. Sci. 26 (1996) p.395.
[91] F. Hooge, Physica B+ C 83 (1976) p.14.
[92] P. Dutta and P. Horn, Rev. Mod. Phys. 53 (1981) p.497.
[93] K.K. Hung, P.K. Ko, C. Hu, Y.C. Cheng, IEEE Trans Electron Devices 37 (1990) p.654.
[94] M.J. Deen, M. Levinshtein, S. Rumyantsev and J. Orchard-Webb, J. Semicond. Sci. Technol. 14 (1999) p.298.
[95] B. Pellegrini, Eur. Phys. J. B 86 (2013) p.1.
[96] B. Pellegrini, P. Marconcini, M. Macucci, G. Fiori and G. Basso, J. Stat. Mech. Theor. Exp 2016 (2016) p.054017.
[97] S. Takeshita, S. Matsuo, T. Tanaka, S. Nakaharai, K. Tsukagoshi, T. Moriyama, T. Ono, T. Arakawa and K. Kobayashi, Appl. Phys. Lett. 108 (2016) p.103106.
[98] E. Rossi, J.H. Bardarson, M.S. Fuhrer and S. Das Sarma, Phys. Rev. Lett. 109 (2012) p.096801.
[99] A. Rahman, J.W. Guikema and N. Marković, Phys. Rev. B 89 (2014) p.235407.
[100] V. Skákalová, A.B. Kaiser, J.S. Yoo, D. Obergfell and S. Roth, Phys. Rev. B 80 (2009) p.153404.
[101] Y. Matsuda, W.-Q. Deng and W.A. Goddard III, J. Phys. Chem. C 114 (2010) p.17845.
[102] J.T. Smith, A.D. Franklin, D.B. Farmer and C.D. Dimitrakopoulos, ACS Nano 7 (2013) p.3661.
[103] L. Wang, I. Meric, P. Huang, Q. Gao, Y. Gao, H. Tran, T. Taniguchi, K. Watanabe, L. Campos, D. Muller, et al., Science 342 (2013) p.614.
[104] L. Vandamme, J. Appl. Phys. 45 (1974) p.4563.
[105] S.M. Song and B.J. Cho, Carbon Lett. 14 (2013) p.162.
[106] C. Gong, S. McDonnell, X. Qin, A. Azcatl, H. Dong, Y.J. Chabal, K. Cho and R.M. Wallace, ACS Nano 8 (2014) p.642.
[107] H. Murrmann and D. Widmann, IEEE Trans. Electron Devices 16 (1969) p.1022.
[108] K.L. Grosse, M.-H. Bae, F. Lian, E. Pop and W.P. King, Nat. Nanotechnol. 6 (2011) p.287.
[109] K. Nagashio, T. Nishimura, K. Kita and A. Toriumi, Appl. Phys. Lett. 97 (2010) p.143514.
[110] Q. Wang, X. Tao, L. Yang and Y. Gu, Appl. Phys. Lett. 108 (2016) p.103109.
[111] H. Yuan, G. Cheng, S. Yu, A.R.H. Walker, C.A. Richter, M. Pan and Q. Li, Appl. Phys. Lett. 108 (2016) p.103505.
[112] X. Li, W. Cai, J. An, S. Kim, J. Nah, D. Yang, R. Piner, A. Velamakanni, I. Jung, E. Tutuc, et al., Science 324 (2009) p.1312.
[113] M.Z. Hasan and J.E. Moore, arXiv preprint arXiv:1011.5462v1 (2010).
[114] G. Gupta, M.B.A. Jalil and G. Liang, Sci. Rep. 4 (2014) p.6220.
[115] Y. Hor, A. Richardella, P. Roushan, Y. Xia, J. Checkelsky, A. Yazdani, M. Hasan, N. Ong and R. Cava, Phys. Rev. B 79 (2009) p.195208.
[116] H.M. Benia, C. Lin, K. Kern and C.R. Ast, Phys. Rev. Lett. 107 (2011) p.177602.
[117] P. Dato and H. Kohler, J. Phys. C: Solid State Phys. 17 (1984) p.3711.
[118] A. Taskin, Z. Ren, S. Sasaki, K. Segawa and Y. Ando, Phys. Rev. Lett. 107 (2011) p.016801.
[119] Z. Ren, A. Taskin, S. Sasaki, K. Segawa and Y. Ando, Phys. Rev. B 84 (2011) p.165311.

[120] G. Yin, D. Wickramaratne, Y. Zhao and R.K. Lake, Appl. Phys. Lett. 105 (2014) p.033118.
[121] Y. Zhang, K. He, C.-Z. Chang, C.-L. Song, L.-L. Wang, X. Chen, J.-F. Jia, Z. Fang, X. Dai, W.-Y. Shan, et al., Nat. Phys. 6 (2010) p.584.
[122] C.-X. Liu, H. Zhang, B. Yan, X.-L. Qi, T. Frauenheim, X. Dai, Z. Fang and S.-C. Zhang, Phys. Rev. B 81 (2010) p.041307.
[123] H.-Z. Lu, W.-Y. Shan, W. Yao, Q. Niu and S.-Q. Shen, Phys. Rev. B 81 (2010) p.115407.
[124] E. Rossi, J. Bardarson, M. Fuhrer and S.D. Sarma, Phys. Rev. Lett. 109 (2012) p.096801.
[125] D.O. Scanlon, P. King, R. Singh, A. De La Torre, S.M. Walker, G. Balakrishnan, F. Baumberger and C. Catlow, Adv. Mater. 24 (2012) p.2154.
[126] J.P. Cascales, I. Martínez, F. Katmis, C.-Z. Chang, R. Guerrero, J.S. Moodera and F.G. Aliev, Appl. Phys. Lett. 107 (2015) p.252402.
[127] X. Xie, D. Sarkar, W. Liu, J. Kang, O. Marinov, M.J. Deen and K. Banerjee, ACS Nano 8 (2014) p.5633.
[128] J. Kang, W. Liu, D. Sarkar, D. Jena and K. Banerjee, Phys. Rev. X 4 (2014) p.031005.
[129] W. Liu, J. Kang, D. Sarkar, Y. Khatami, D. Jena and K. Banerjee, Nano Lett. 13 (2013) p.1983.
[130] D. Ovchinnikov, A. Allain, Y.-S. Huang, D. Dumcenco and A. Kis, ACS Nano 8 (2014) p.8174.
[131] S. Kogan, *Electronic Noise and Fluctuations in Solids*, Cambridge University Press, Chicago, 2008.
[132] L.B. Kiss and P. Svedlindh, Phys. Rev. Lett. 71 (1993) p.2817.
[133] A.S. Tremblay, S. Feng and P. Breton, Phys. Rev. B 33 (1986) p.2077.
[134] S. Najmaei, Z. Liu, W. Zhou, X. Zou, G. Shi, S. Lei, B.I. Yakobson, J.-C. Idrobo, P.M. Ajayan and J. Lou, Nat. Mater. 12 (2013) p.754.
[135] A.M. van der Zande, P.Y. Huang, D.A. Chenet, T.C. Berkelbach, Y. You, G.-H. Lee, T.F. Heinz, D.R. Reichman, D.A. Muller and J.C. Hone, Nat. Mater. 12 (2013) p.554.
[136] O.V. Yazyev and S.G. Louie, Nat. Mater. 9 (2010) p.806.
[137] N.M.R. Peres, F. Guinea, and A.H. Castro Neto, Phys. Rev. B. 73 (2006), p.125411.
[138] A. Mesaros, S. Papanikolaou, C.F.J. Flipse, D. Sadri and J. Zaanen, Phys. Rev. B 82 (2010) p.205119.
[139] Z. Zhang, X. Zou, V.H. Crespi and B.I. Yakobson, ACS Nano 7 (2013) p.10475.
[140] D. Sharma, M. Amani, A. Motayed, P.B. Shah, A.G. Birdwell, S. Najmaei, P.M. Ajayan, J. Lou, M. Dubey, Q. Li, et al., Nanotechnology 25 (2014) p.155702.
[141] L. Li, Y. Yu, G.J. Ye, Q. Ge, X. Ou, H. Wu, D. Feng, X.H. Chen and Y. Zhang, Nat. Nanotechnol. 9 (2014) p.372.
[142] K.R. Amin and A. Bid, Appl. Phys. Lett. 106 (2015) p.183105.
[143] K.R. Amin and A. Bid, ACS Appl. Mater. Interfaces 7 (2015) p.19825.
[144] A. Kuc, N. Zibouche and T. Heine, Phys. Rev. B 83 (2011) p.245213.
[145] Data available at https://en.wikipedia.org/w/index.php?title=Transistor_count&oldid=754563608
[146] S. Ghatak, A.N. Pal and A. Ghosh, ACS Nano 5 (2011) p.7707.
[147] A. Figueroa, G. van der Laan, L. Collins-McIntyre, S.-L. Zhang, A. Baker, S. Harrison, P. Schönherr, G. Cibin and T. Hesjedal, Phys. Rev. B 90 (2014) p.134402.
[148] S. Shamim, S. Mahapatra, C. Polley, M.Y. Simmons and A. Ghosh, Phys. Rev. B 83 (2011) p.233304.
[149] D. Tobias, M. Ishigami, A. Tselev, P. Barbara, E.D. Williams, C.J. Lobb and M.S. Fuhrer, Phys. Rev. B 77 (2008) p.033407.
[150] E. Simoen and C. Claeys, Solid-State Electron 43 (1999) p.865.